EurJIC
European Journal of Inorganic Chemistry

Research Article
doi.org/10.1002/ejic.202300102

Chemistry Europe
European Chemical Societies Publishing

www.eurjic.org

Deep Red Emitting Heteroleptic Ir(III) Complexes that Incorporate Unsymmetrical 4-quinoline Carboxylic Acid Derived Ligands

Christopher E. Elgar,[a] Haleema Y. Otaif,[a] Joseph M. Beames,[a] Peter N. Horton,[b] Simon J. Coles,[b] Andrew J. Hallett,[c] Sean P. O'Kell,[c] and Simon J. A. Pope*[a]

Six disubstituted ligands based upon 2-(2′-pyridinyl/pyrazinyl)quinoline-4-carboxylic acids have been synthesised, solvent-free, in one step from a range of commercially available isatin derivatives. These species behave as ancillary chelating ligands for Ir(III) complexes of the form $[Ir(C\text{^}N)_2(N\text{^}N)]PF_6$ (where C^N = cyclometalating ligand; N^N = 2-(2′-pyridinyl/pyrazinyl)quinoline-4-carboxylic acids). An X-ray crystallographic study on one complex shows a distorted octahedral geometry wherein a *cis*-C,C and *trans*-N,N coordination mode is observed for the cyclometalating ligands. DFT calculations predicted that variations in N^N ligand from 2,2′-bipyridine to $\mathbf{L^{1-6}}$ should localise the LUMO on to the $\mathbf{L^n}$ ligand and that the complexes are predicted to display MLCT/LLCT character. All complexes displayed luminescence in the deep red part of the visible region (674–679 nm) and emit from triplet states, but with little apparent tuning as a function of $\mathbf{L^{1-6}}$. Further time-resolved transient absorption spectroscopy supports the participation of these triplet states to the excited state character.

Introduction

Luminescent metal complexes based on organometallic iridium(III) species have demonstrated major applications in optoelectronic and photonic disciplines.[1] The myriad variants of these complexes have been successfully used in diverse areas of research, such as bioimaging,[2] electroluminescence,[3] photoredox catalysts,[4] non-linear optics,[5] chemosensors,[6] and energy upconversion.[7] Underpinning the successful deployment of Ir(III) species within these disciplines implies a need to understand the inherent electronic characteristics of such complexes.[8] Both the design and subsequent combination of ligands at Ir(III)[9] is essential to control and tune such properties.[10]

One of the most intensely studied classes of Ir(III) complex are the cationic, heteroleptic species $[Ir(C\text{^}N)_2(L\text{^}L)]^{n+}$ (where C^N = cyclometalating ligand; L^L = chelating ligand).[11] These compounds can be synthesised via the step-wise addition of ligands to the Ir(III) centre which can then allow exquisite control over the resultant electronic properties.[12]

In $[Ir(C\text{^}N)_2(L\text{^}L)]^{n+}$ type complexes it is well known that both ligands can influence the HOMO and LUMO levels that determine photoluminescence behaviour. For example, for the archetypal complex $[Ir(ppy)_2(bipy)]^+$ (where ppy = 2-phenylpyridine, bipy = 2,2′-bipyridine) the important LUMO level(s) are located on the ancillary diimine ligand.[12] The luminescence properties can therefore be tuned by modulating the energy of the LUMO level via the diimine structure (e.g. using substituents). In contrast, our own studies have investigated $[Ir(2\text{-}pqx)_2(bipy)]^+$ (where 2-pqx = 2-phenylquinoxaline derivative)[13,14] where the cyclometalated 2-pqx ligand contributes strongly to the important HOMO and LUMO energies, whilst the diimine is essentially a spectator ligand. The advantage of this approach is that precise tuning of emission can thus be controlled through the details of the 2-pqx ligand, and the diimine ligand can be used to introduce other functionality, for example targeting vectors for directed bioimaging studies.[15] The design of Ir(III) complexes has now advanced to the stage where deep-red to near-IR emissive systems have been reported through the use of highly conjugated cyclometalating ligands.[16]

In this study, we firstly describe the synthesis of unsymmetrical, disubstituted mixed-donor diimine ligands (Scheme 1) related to the 2-(2′-pyridyl)quinoline core structure. In comparison to ubiquitous 2,2′-bipyridines,[17] 2-(2′-pyridyl)quinolines have been far less studied in coordination chemistry, but reports include both bidentate N,N[18] and "roll-over" cyclometalation C,N modes.[19] The new ligands described herein also feature several sites of substitution (Scheme 1) and incorporate a 4-quinoline carboxylic acid motif. As an aside, derivatives of 4-quinoline carboxylic acids have been widely investigated as biologically active agents, including as inhibitors of dihydroor-

[a] Dr. C. E. Elgar, H. Y. Otaif, Dr. J. M. Beames, Prof. S. J. A. Pope
School of Chemistry, Main Building,
Cardiff University
Cardiff, CF10 3AT, Cymru/Wales (UK)
E-mail: popesj@cardiff.ac.uk
[b] Dr. P. N. Horton, Prof. S. J. Coles
UK National Crystallographic Service, Chemistry,
University of Southampton
Highfield, Southampton, SO17 1BJ, (UK)
[c] Dr. A. J. Hallett, Dr. S. P. O'Kell
STG Aerospace
Brecon House, Cwmbran, NP44 3AB (UK)

Supporting information for this article is available on the WWW under https://doi.org/10.1002/ejic.202300102

Research Article
doi.org/10.1002/ejic.202300102

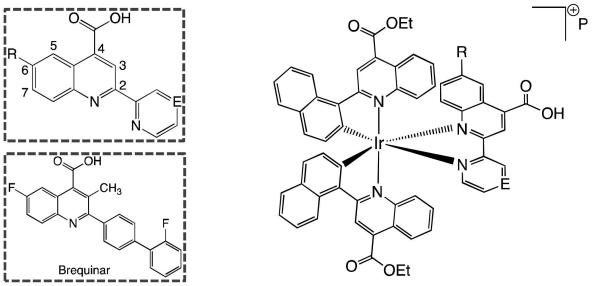

Scheme 1. General structure of the heteroleptic Ir(III) complexes investigated in this study (E=C, N; R=H, OMe, F). Numbering scheme for the quinoline ring shown inset, together with the molecular structure of Brequinar®.

otate dehydrogenase,[20] and also as promising anti-cancer agents, including Brequinar®[21] (shown in Scheme 1), which has undergone phase II clinical trials for a variety of cancers.[22] Recent studies of 4-quinoline carboxylic acids have also demonstrated potency as novel SIRT3 inhibitors for the possible treatment of leukemia.[23]

In addition to the development of novel ligands, we also report their incorporation into cationic, heteroleptic Ir(III) species, $[Ir(C^N)_2(N^N)]^+$. These complexes possess a 2-(1-naphthyl)quinoline[24] ligand as cyclometalating (C^N) agent, and the 4-quinoline carboxylic acid derivatives as bidentate N,N chelates. The Ir(III) complexes were shown to be luminescent in the deep-red spectral region.

Results and Discussion

Synthesis

A series of substituted 2-(2′-pyridinyl/pyrazinyl)-quinoline-4-carboxylic acids (**L**$^{1-6}$) were conveniently synthesised following a modified Pfitzinger methodology (Scheme 2),[25] although other routes have been explored.[26] Briefly, the solid 5-subsitituted isatin and an equimolar amount of either 2-acetylpyridine, or 2-acetylpyrazine, was added to a pestle and mortar and ground together in a solvent-free manner (see Experimental section for details). The ligands were subsequently obtained as air stable powders in moderate to good yields. Of the isolated species, only **L**^{1}[27] and **L**^{4}[28] have been previously reported in the literature, and neither have been investigated as ligands.

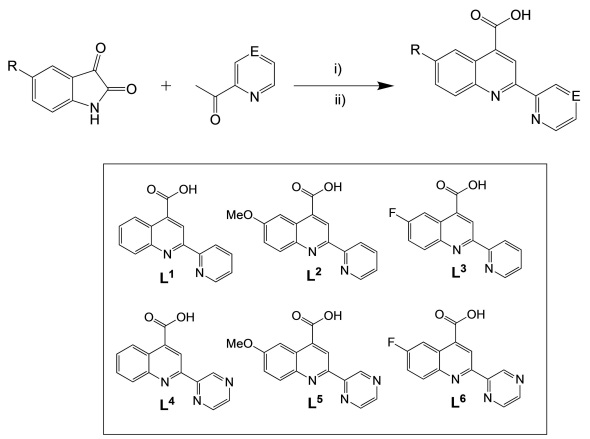

Scheme 2. The synthetic route towards the new diimine ligands (inset). Reagents and conditions: i) 33% $NaOH_{(aq)}$ (4 equiv.), room temperature. ii) H_2O, HCl (5 M).

In the ^{1}H NMR spectra (measured in d_6-DMSO), each of the ligands (**L**$^{1-6}$) displayed a singlet centred around 9.0 ppm which was assigned to the proton in the 3-position of the quinoline ring (Figures S1–S7). The pyrazine containing ligands **L**$^{4-6}$ all showed a singlet resonance between 9.7 and 9.8 ppm assigned to the 3-position of the pyrazine ring. In most cases a broad $-CO_2H$ resonance was also observed ca. 14 ppm. The $^{19}F\{^1H\}$ NMR spectra for **L**^{3} and **L**^{6} showed a singlet peak at −110.0 and −109.1 ppm respectively, consistent with an aromatic fluorine environment (Figures S4 and S8). Satisfactory HRMS data were obtained for each new ligand.

The iridium complexes were synthesised using **L**$^{1-6}$ as ancillary N^N ligands (Scheme 3).[29] Briefly, a slight molar excess of **L**$^{1-6}$ was added to a stirring chloroform solution of *cis*-$[Ir(1nq)_2(MeCN)_2]BF_4$ (where 1nq = 2-(naphthalen-1-yl)quinoline-4-carboxylate ethyl ester). Complexes were initially obtained as their BF_4^- salts and purified via silica gel chromatography, eluting first with 95:5 DCM/MeOH to remove the precursor complex, before eluting the desired complex as a red band using 9:1 DCM/MeOH. BF_4^-/PF_6^- anion exchange was performed for $[Ir(1nq)_2(\mathbf{L}^1)]^+$ to help promote crystallisation. All complexes were isolated as air stable solids.

General Characterisation of the Complexes

The complexes were characterised by ^{1}H, $^{19}F\{^1H\}$, $^{13}C\{^1H\}$ NMR, UV-vis. absorption, emission, and IR spectroscopies, as well as HRMS. For the ^{1}H NMR spectra a number of observations confirmed formation of the complexes. Firstly, it was interesting to note that the methoxy groups from **L**^{2} and **L**^{5} shifted upfield upon complexation with Ir(III) (from 3.94 and 3.93 ppm, to 3.66 ppm and 3.85 ppm, respectively). The unsymmetrical nature of the ancillary ligand renders both cyclometalating ligands as inequivalent leading to complex, but well resolved

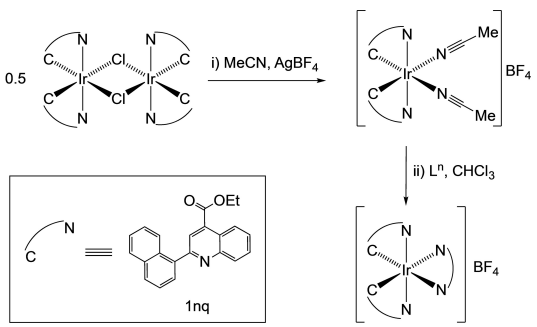

Scheme 3. The synthetic route to the complexes (cyclometalating ligand, 1nq, shown inset).

Research Article
doi.org/10.1002/ejic.202300102

spectra, particularly in the aromatic region (Figures S9–S15). In addition, the ethyl groups become inequivalent with a clear distinction noted in the chemical shifts of the aliphatic coupling (triplet and quartet) patterns.

The complexes of **L**$^{4-6}$ revealed the most downfield resonance was associated with the pyrazine moiety *ca.* 9.5–9.6 ppm. The 3-position proton on the ancillary quinoline was observed at *ca.* 8.0 and 8.1 ppm for the pyridine and pyrazine complexes respectively. The singlet resonance from one of the cyclometalated quinoline 3-position appeared *ca.* 9.3 ppm for both pyridine and pyrazine complexes. In the second cyclometalating ligand, the 3-position proton signal is much more upfield, with the resonance appearing *ca.* 8.2 ppm for the pyridine complexes and 8.4 ppm for the pyrazine complexes. As discussed later, the solid-state single crystal structure of [Ir(1nq)$_2$(**L**^{2})]PF$_6$ revealed a significant amount of strain in one of the cyclometalating ligands. The proton centroid distances between the 3-position protons and the opposite quinoline aromatic ring are ca. 3.51 and 3.79 Å, implying the proton is within range to experience extra shielding and thus a relative upfield shift.

The effect of the intra-ligand strain was also evident in the proton environments *ortho* to the Ir–C coordinate bond. [Ir(1nq)$_2$(**L**^{n})]$^+$ has one doublet between 7.02–7.08 ppm ($^3J_{HH}$ between 8.2–8.5 Hz), and a second doublet was much more shielded around 6.3 ppm ($^3J_{HH}$ between 8.3–8.6 Hz). For reference, [Ir(1nq)$_2$(bipy)]PF$_6$ (where both C^N ligands are equivalent) shows one doublet at 6.99 ppm ($^3J_{HH}$ = 8.4 Hz) in $CDCl_3$. ^{1}H-^{1}H COSY correlation spectroscopy obtained for [Ir(1nq)$_2$(**L**^{1})]PF$_6$ revealed that this doublet is position 8 of a naphthyl ring.

^{19}F{^{1}H} NMR spectra were also obtained for complexes of **L**^{3} and **L**^{6} and revealed that upon complexation the singlet resonance became more deshielded (to −108.0 and −102.5 ppm, respectively). The magnitude in the change of the chemical shift was smaller for **L**^{3}. Finally, high-resolution mass spectrometry data provided a *m/z* peak and isotopic distribution as expected for the cationic complex fragment [M]$^+$ in each case.

X-ray Structural Study

Dark red, cut-blade crystals of [Ir(1nq)$_2$(**L**^{1})]PF$_6$ (Figure 1) were successfully grown from vapour diffusion of diisopropyl ether into a chloroform solution of the complex, and investigated by single crystal X-ray diffraction. For [Ir(1nq)$_2$(**L**^{1})]PF$_6$, no solvent masking was used, however a molecule of diisopropyl ether and a disordered chloroform molecule, H-bonded to a ligand and anion respectively, are present in the asymmetric unit (Figure 1). The structure displayed the expected coordination with a *cis*-C,C and *trans*-N,N arrangement of the cyclometalating ligands around the distorted octahedral iridium(III) centre. The principal bond lengths and angles that describe the coordination sphere (Table S1, Supporting Information) all fall within the expected range as noted in previous examples,[30] and especially those with aryl–quinoline ligands at Ir(III).[31]

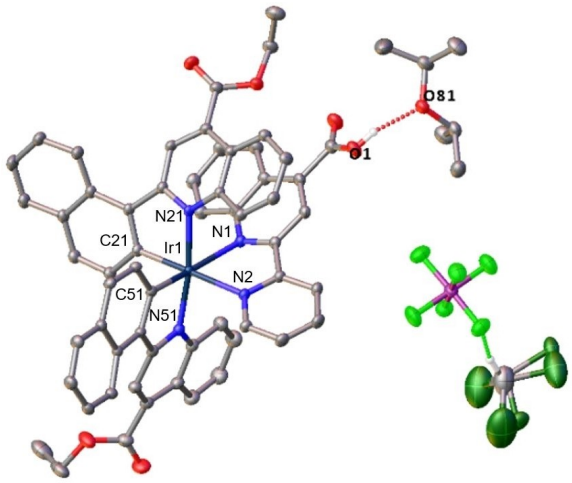

Figure 1. X-ray structure of [Ir(1nq)$_2$(**L**^{1})]PF$_6$ showing H-bonding interactions between solvent and complex (≤ 2.84 Å). Structure details: $C_{66}H_{57}Cl_3F_6IrN_4O_7P$, M_r = 1461.67, triclinic, P-1 (No. 2), a = 13.11880(10) Å, b = 15.6022(2) Å, c = 16.0146(2) Å, α = 70.1570(10)°, β = 83.6410(10)°, γ = 74.2860(10)°, V = 2967.41(6) Å^3, T = 100(2) K, Z = 2, Z′ = 1, μ(Mo K$_\alpha$) = 2.491 mm^{-1}, 237955 reflections measured, 18055 unique (R_{int} = 0.0551) which were used in all calculations. The final wR_2 was 0.0670 (all data) and R_1 was 0.0261 (I > 2(I)).

The packing diagram (Figure 2) shows that intermolecular pi-stacking is evident between neighbouring cationic units. The dominant interaction is between the quinoline rings of the 1nq ligands of neighbouring complexes. The structure also reveals significant distortions within the different ligands. The N–C–C–N angles of **L**^{1} (i.e. the degree of rotation between the two heterocyclic rings) is 20.1(3)°, which is significantly larger

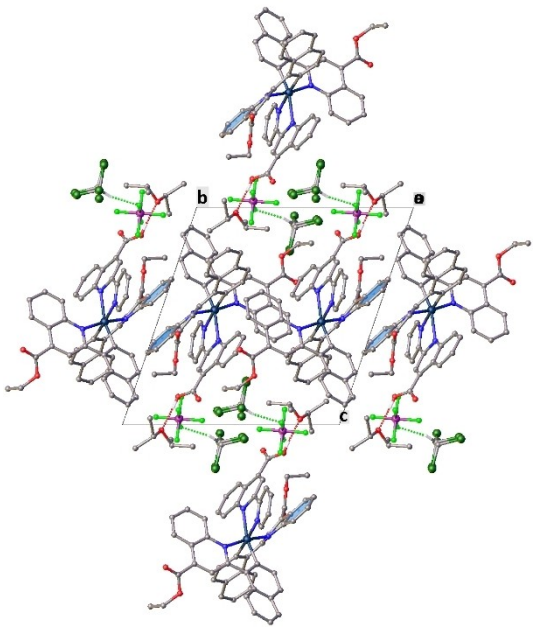

Figure 2. Packing diagram of [Ir(1nq)$_2$(**L**^{1})]PF$_6$ exhibits π–π interactions between aromatic rings highlighted in blue.

Research Article
doi.org/10.1002/ejic.202300102

than the 6.2(5)° observed for bipy in $[Ir(1nq)_2(bipy)]PF_6$. The large distortions observed in the cyclometalating ligands is closely comparable to that observed for $[Ir(1nq)_2(bipy)]PF_6$ (Figure S16 and Table S2). In $[Ir(1nq)_2(\mathbf{L^1})]PF_6$, the intraligand deformation of $\mathbf{L^1}$ is towards the cyclometalating ligand and thus reduces the proton-ring centroid distances between the two quinoline C3-position protons and the opposite quinoline aromatic ring to ca. 3.5 Å and 3.8 Å (see earlier discussion of the NMR spectra). The ligand deformations also lead to a shortening of the distance between the ester group $-CH_2$ moiety on 1nq and the carbonyl of the $-CO_2H$ group on $\mathbf{L^1}$.

Density Functional Theory

Density functional theory (DFT) calculations were performed on each of the complexes to probe the electronic characteristics and help inform the discussion of the electronic transitions. All calculations were undertaken using the B3LYP functional with a 6-31G* basis set, and an SDD ECP for the central iridium atom. Calculations were performed within an implicit acetonitrile solvent, consistent with the spectroscopic measurements.

Geometries of the complexes were optimised using the prior method, and the resulting minimum energy (Table S3) structures were compared against the X-ray crystallographic data to demonstrate the suitability of the method. The geometrical structures obtained from the DFT optimisations for $[Ir(1nq)_2(\mathbf{L^n})]^+$ are in reasonable agreement with the crystallographic data (Table 1 and Figure 3).

Firstly, molecular orbital decomposition analysis was performed on each complex. This method (Table 2) predicted that the HOMO was composed of contributions from the 5d orbital of the iridium centre (17–19%) and each cyclometalated ligand (ca. 80% in total), and a negligible contribution from $\mathbf{L^n}$ (1%). The LUMO was predicted to be dominated (91–96%) by $\mathbf{L^n}$ character (see also Figures 4 and S18–S22). This is very different from the calculations for $[Ir(1nq)_2(bipy)]^+$ where the LUMO character was dominated by the cyclometalated 1nq ligands; the bipy ligand was only predicted to contribute to the higher energy LUMO+2 and LUMO+3.[24] Therefore, the calculations suggest that the change from bipy to $\mathbf{L^n}$ may alter the ordering of the LUMOs across the different ligands. As noted earlier, this predicts behaviour more comparable to $[Ir(ppy)(bipy)]^+$ type complexes.[12] The two 1nq/1nq′ ligands form pairs of pseudo-degenerate orbitals with alternating contributions from each LUMO+1 and LUMO+2. The metal contribution to the unoccupied orbitals is negligible. Taken together these calculations predict that the singlet excited states may have a significant mixture of $ligand_{(1nq)}$-to-$ligand_{(N^\wedge N)}$ charge transfer (LLCT), $intraligand_{(1nq)}$ charge transfer (ILCT) and metal-to-ligand charge transfer (MLCT) character.

To estimate the vertical excitation energies of the low-lying singlet and triplet excited states of the complexes, TD-DFT calculations using the CAM-B3LYP functional were carried out from the optimised ground-state geometries. In each case, the lowest 30 singlet-to-singlet spin-allowed and 30 singlet-to-triplet spin-forbidden transitions were calculated. The non-relativistic nature of the calculations means that the spin-allowed transitions were prioritised, but the spin-forbidden excitation energies can also be used to propose absorption band character. The calculated transitions were in reasonable agreement with the experimental absorption spectra discussed later (Table 3, Figure S17).

In the case of $[Ir(1nq)_2(\mathbf{L^1})]^+$, the lowest spin-allowed $S_o \rightarrow S_1$ transition was predicted to occur at ca. 440 nm and correlated well with the broad, structureless feature observed in the

Table 1. Comparison of the experimental coordination sphere M–L bond lengths of $[Ir(1nq)_2(\mathbf{L^1})]^+$ with those obtained from the calculated optimised geometry.

Bond	Calculated	Experimental
Ir1 N1	2.379 Å	2.2836(17) Å
Ir1 N2	2.227 Å	2.1476(17) Å
Ir1 N21	2.136 Å	2.0973(17) Å
Ir1 N51	2.131 Å	2.0751(18) Å
Ir1 C21	2.030 Å	2.0194(19) Å
Ir1 C51	2.004 Å	1.9834(19) Å

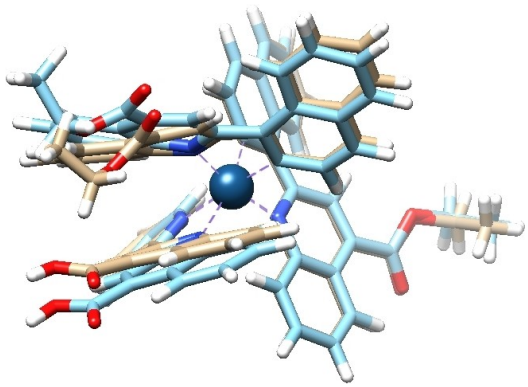

Figure 3. Overlay of the crystal structure (blue) and DF-DFT//B3LYP/6-31G*-(SDD) optimised structures (brown) for $[Ir(1nq)_2(\mathbf{L^1})]^+$. The structures exhibit a root-mean-square deviation (RMSD) of 0.3 a.

Table 2. A summary of the major calculated contributions (%) to each MO from each part of the complex. 1nq and 1nq′ are the inequivalent C^N ligands.

Complex	Ir HOMO	1nq HOMO	LUMO	LUMO+1	1nq′ HOMO	LUMO	LUMO+1	L^n LUMO
L^1	19	48	4	70	33	1	23	93
L^2	19	48	5	39	32	1	55	91
L^3	18	49	3	46	31	1	46	93
L^4	18	48	2	60	33	1	34	94
L^5	17	49	3	78	33	1	14	96
L^6	18	48	2	61	33	1	32	94

Research Article
doi.org/10.1002/ejic.202300102

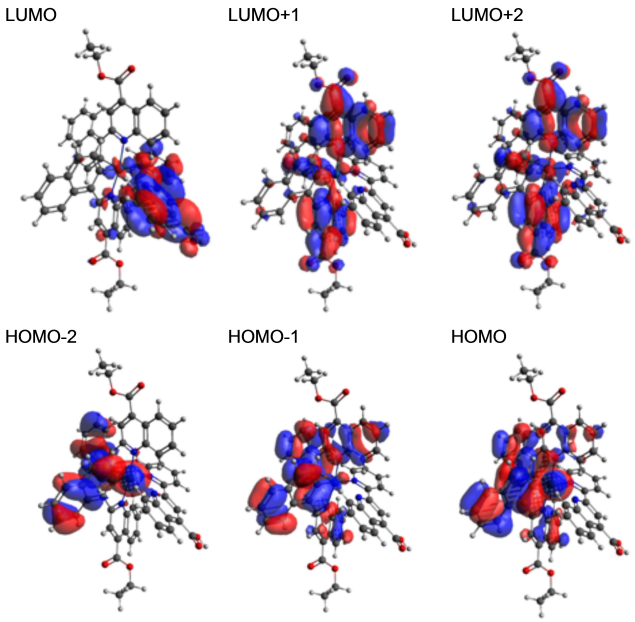

Figure 4. Calculated Kohn-Sham molecular orbitals for $[Ir(1nq)_2(\mathbf{L^1})]^+$. Calculated spin densities are reported in Supporting Information.

Table 3. Calculated energies for the transitions between the ground state and excited states for each of the complexes.

Complex	$S_0 \rightarrow S_1$ (nm)	$S_o \rightarrow T_1$ (nm)	$T_1 \rightarrow S_0$ (nm) (adiabatic)
$[Ir(1nq)_2(L^1)]^+$	440	639	713
$[Ir(1nq)_2(L^2)]^+$	439	640	712
$[Ir(1nq)_2(L^3)]^+$	441	641	713
$[Ir(1nq)_2(L^4)]^+$	441	640	712
$[Ir(1nq)_2(L^5)]^+$	439	641	711
$[Ir(1nq)_2(L^6)]^+$	443	640	712

experimental absorption spectrum with molar absorption values approximately 5000 $M^{-1}cm^{-1}$. The calculated wavelength of the spin forbidden $S_o \rightarrow T_1$ transition seemed to be slightly over-estimated at 639 nm, which probably correlates with the long tail of the lowest energy absorption feature in the experimental data. In both types of transition, the calculations suggest very little change in energy as $\mathbf{L^n}$ is varied.

The most important singlet transitions of $[Ir(1nq)_2(\mathbf{L^1})]^+$ and their associated oscillator strengths and configurations are summarised in Table S4, with analogous data for $[Ir(1nq)_2(\mathbf{L^{2-6}})]^+$ shown in Tables S5–S9. The longest wavelength singlet excitation is expected to be intense HOMO→LUMO (31%) and HOMO→LUMO+1 (35%) transitions at 440 nm, followed by an intense transition at 422 nm comprised of roughly equal contributions of HOMO→LUMO+1/LUMO+2 and HOMO-1→LUMO+1.

The TD-DFT calculations therefore predicted that the variations in $\mathbf{L^n}$ (through changes in both substituents and heterocycle) may not induce a substantial modulation of the electronic properties of the complexes.

Absorption and Emission Properties

The electronic properties of the complexes were studied using a variety of experimental techniques. Absorption spectra for the complexes of $[Ir(1nq)_2(\mathbf{L^{1-6}})]^+$ were obtained in aerated MeCN solution at 10^{-5} M (Figure 5, Table 4) where the spectra are compared to $[Ir(1nq)_2(bipy)]PF_6$.[24] All six complexes showed strong absorbances between 200 nm and 400 nm, occurring from the various $\pi \rightarrow p^*$ transitions inherent to the different aromatic constituents of the ligands (as indicated by DFT). The free ligands do not possess absorption >400 nm (Figure S17), and therefore the new features around 450–550 nm (ε values *ca.* 4000–6000 $M^{-1}cm^{-1}$) are assigned to the different types of spin allowed CT transitions (including MLCT, ILCT and LLCT) predicted by DFT; the weaker, spin forbidden CT transitions may contribute >550 nm.[24] The subtle structural differences associated with the ancillary ligands do impart differences in the appearance and intensity of the ligand-based transitions, but the general features appear relatively unperturbed. Certainly, the region at 450–550 nm, which is likely to contain significant MLCT character, look very similar for each complex.

Room temperature luminescence data (Table 4) on MeCN solutions of the complexes utilised an excitation wavelength of

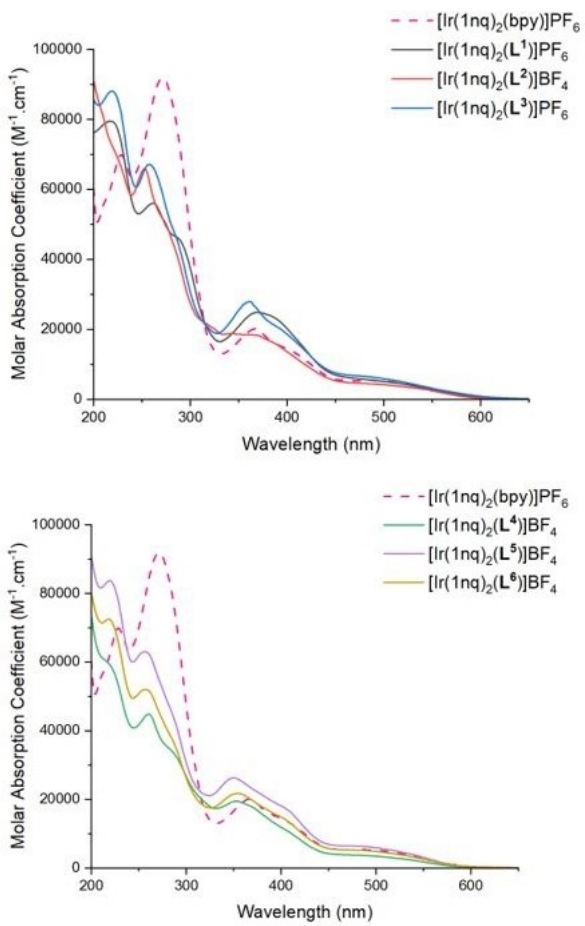

Figure 5. A comparison of the UV-vis. absorption spectra for $[Ir(1nq)_2(\mathbf{L^n})]^+$ obtained in MeCN solution at ca. 10^{-5} M.

Research Article
doi.org/10.1002/ejic.202300102

Table 4. Absorbance and emission data for the complexes at room temperature[a]

Complex	λ_{abs} ($\varepsilon \times 10^4$ $M^{-1}cm^{-1}$)/ nm	λ_{em}/nm[b]	τ/ns[c]	Φ [d]
$[Ir(1nq)_2(L^1)]PF_6$	494 (0.5), 373 (2.4), 285 (4.6), 261 (5.6), 217 (7.9)	678	411 (985)	0.03
$[Ir(1nq)_2(L^2)]PF_6$	492 (0.5), 368 (1.8), 273(sh) (5.0)	679	268 (866)	0.02
$[Ir(1nq)_2(L^3)]PF_6$	490 (0.6), 391 (2.0), 361 (2.8), 257 (6.6), 219 (8.8)	679	275 (985)	0.02
$[Ir(1nq)_2(L^4)]PF_6$	492 (0.4), 402(sh) (1.1), 356(br) (1.9), 282 (3.5), 260 (4.5), 217 (6.0)	674	323 (1212)	0.03
$[Ir(1nq)_2(L^5)]PF_6$	493 (0.6), 404(sh) (1.7), 349 (2.6), 256 (6.3), 219 (8.4)	677	385 (1151)	0.03
$[Ir(1nq)_2(L^6)]PF_6$	495 (0.5), 396(sh) (1.5), 355 (2.2), 256 (5.1), 218 (7.3)	673	313 (1207)	0.02

[a] All measurements in aerated MeCN unless otherwise stated. b 355 nm or 510 nm excitation; c 355 nm excitation, values in parentheses are deoxygenated solutions; d referenced against 0.018 for $[Ru(bpy)_3][PF_6]_2$ in aerated MeCN.[32]

510 nm (selective for the longest wavelength absorption band) and showed an emission around 680 nm with a featureless band profile which is typical of an emitting state with significant CT character (Figure 6). For reference, $[Ir(1nq)_2(bipy)]^+$ emits at 679 nm. Therefore, despite the different structures of the ancillary ligands, $\mathbf{L^{1-6}}$, there was little variance in the position of the emission maxima as a function of the ancillary diimine: this experimental data confirmed the predictions of the DFT calculations. These observations are diffferent to more common $[Ir(ppy)_2(N^N)]^+$ complexes where it has been shown that the N^N ancillary ligand can very effectively tune the energy of the LUMO and thus directly modulate the emission properties.[12]

Low temperature (77 K) emission spectra (Figure 6) obtained on 4:1 ethanol/methanol frozen glasses, showed a slight hypsochromic shift (likely due to rigidochromism) to 660 nm, with a variable shoulder feature at lower energy. For the pyridine-containing complexes ($\mathbf{L^{1-3}}$) this shoulder is hypsochromically shifted by ca. 10 nm, from 720 nm to 710 nm; for the pyrazine-containing complexes ($\mathbf{L^{4-6}}$), the shoulder is at a slightly higher energy, 705 nm.

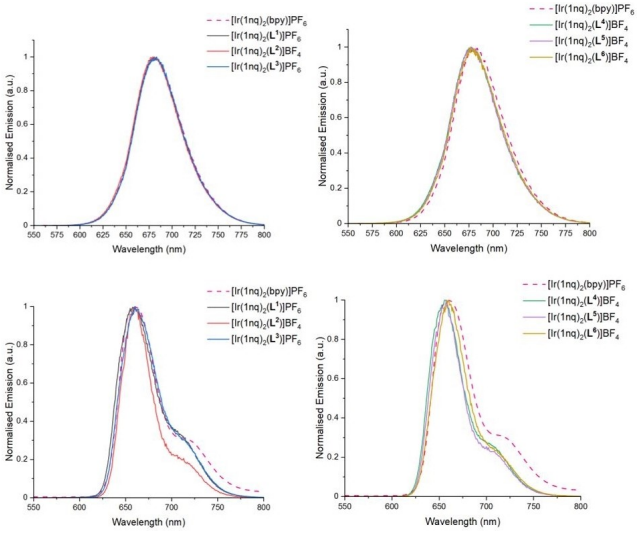

Figure 6. Top: Normalised emission spectra for $[Ir(1nq)_2(\mathbf{L^n})]^+$ obtained in MeCN solution at ca. 10^{-5} M room temeprature. Bottom: Low temperature emission spectra recorded in a MeOH/EtOH (1:4) glass at 77 K ($\lambda_{ex} = 510$ nm in all cases).

Room temperature lifetime values were obtained from the decay kinetics of time-resolved measurements (using pulsed 355 nm excitation) and were in the range 313–411 ns. These values are longer than for the reference compound $[Ir(1nq)_2(bipy)]^+$ (240 ns).[24] Upon deoxygenation of the solutions the lifetime values were extended into the microsecond domain (866–1212 ns) and are therefore consistent with an emitting state that is triplet in nature and likely to contain a dominant CT character.

It is noteworthy that interest in Ir(III)-based red emitters[33] has blossomed in recent years, especially in an effort to address particular applications, such as OLEDs[34] and bioimaging,[35] that can directly benefit from longer wavelength emission character. The long-lived deep red emission demonstrated by these complexes could therefore be considered in such areas of application.

Time resolved transient absorption spectroscopy (TR-TAS)

Nanosecond transient absorption (TA) spectra of all Ir(III) complexes were recorded in aerated acetonitrile using a pump wavelength of 355 nm and are shown in Figure 7. The general spectral appearance of all six complexes is broadly similar, but with some notable differences.

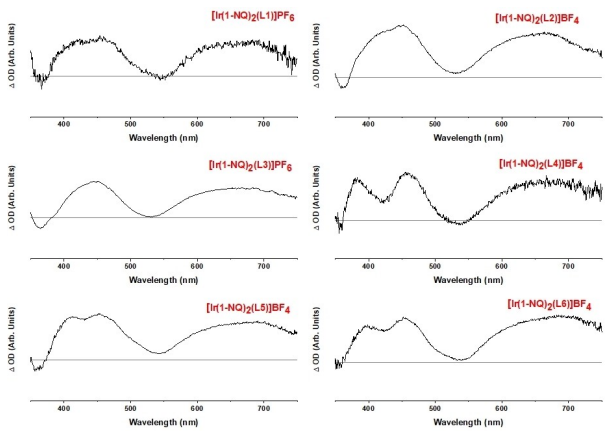

Figure 7. Background and luminescence subtracted transient absorption spectra of all complexes in aerated acetonitrile, $\lambda_{ex} = 355$ nm. The grey line represents $\Delta OD = 0$ in all cases.

Research Article
doi.org/10.1002/ejic.202300102

The complexes all feature a weak ground state bleach in the shorter wavelength spectral region (350 nm $<\lambda<$ 375 nm), ascribed to the pump-driven depletion of the ground state CT absorption band. The spectra also exhibit strong increases in optical density in the regions 375 nm $<\lambda<$ 500 nm and 550 nm $<\lambda<$ 750 nm, assigned to triplet–triplet absorption bands ($T_1 \rightarrow T_n$ transitions) as indicated by the magnitude of the associated lifetime values (Table 5). Across the series of complexes, the shorter wavelength features differ in appearance with two distinct contributions (which share the same decay kinetics) noted for the pyrazine derivatives, $[Ir(1nq)_2(\mathbf{L}^{4-6})]^+$. In contrast, the longer wavelength triplet absorption feature is broad and featureless and tails beyond 700 nm. In all cases the lifetimes of these features (e.g. Figure 8) correlate closely with those obtained through time-resolved emission measurements.

Table 5. Kinetic data obtained from the fitted time-resolved transient absorption spectra aerated acetonitrile of the complexes $[Ir(1nq)_2(\mathbf{L}^n)]^+$, $\lambda_{ex}=355$ nm.

	Lifetime (ns)		Lifetime (ns)
L^1	405 nm (412.6 ± 2.0)	L^4	357 nm (295.3 ± 8.0)
	453 nm (449.6 ± 1.5)		382 nm (355.7 ± 2.0)
	653 nm (426.7 ± 2.4)		460 nm (345.6 ± 1.6)
	678 nm (410.7 ± 0.4)		630 nm (343.8 ± 2.1)
			674 nm (323.5 ± 0.9)
L^2	361 nm (275.9 ± 9.3)	L^5	367 nm (382.8 ± 9.2)
	403 nm (253.3 ± 1.5)		415 nm (356.9 ± 7.5)
	453 nm (263.1 ± 1.6)		475 nm (387.3 ± 3.7)
	651 nm (260.0 ± 0.6)		635 nm (397.3 ± 1.0)
	679 nm (268.2 ± 0.2)		677 nm (364.3 ± 0.7)
L^3	366 nm (253.8 ± 2.9)	L^6	359 nm (309.3 ± 3.9)
	410 nm (271.2 ± 0.9)		385 nm (327.6 ± 3.2)
	650 nm (271.3 ± 0.7)		460 nm (327.7 ± 1.0)
	679 nm (275.6 ± 0.2)		630 nm (330.6 ± 1.2)
			673 nm (313.2 ± 0.4)

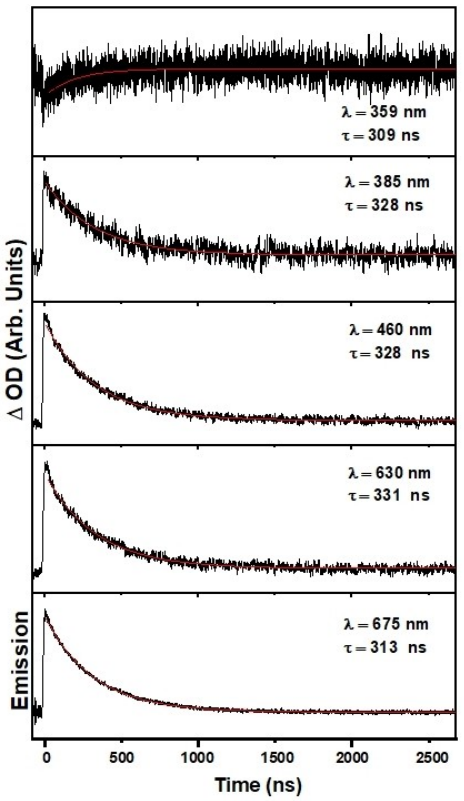

Figure 8. Fitted (red line) kinetic traces of the major features of the transient spectrum of $[Ir(1nq)_2(\mathbf{L}^6)]BF_4$ in acetonitrile at room temperature, aerated. Wavelengths and lifetimes of each trace are inset.

Conclusions

A series of unsymmetrical 2-(2′-pyridinyl/pyrazinyl)quinoline-4-carboxylic acids have been synthesised with either fluorine or methoxy substituents. The ligands were demonstrated to coordinate to Ir(III) yielding heteroleptic, cationic complexes. The X-ray crystal structure of one example showed the expected coordination sphere and confirmed the diimine ligand coordinated in a bidentate N,N fashion. NMR spectroscopic characterisation of the complexes showed the influence of the unsymmetrical ligand as well as evidence for the shielding of particular proton environments that arise due to the intraligand distortions. DFT calculations were deployed to help predict the electronic properties of the complexes. The calculations suggested that the use of the 2-(2′-pyridinyl/pyrazinyl)quinoline-4-carboxylic acid ligands, $\mathbf{L}^{1-6}$, should dictate the LUMO character of the complexes, and give a mixture of MLCT, ILCT and LLCT contributions to the visible absorption bands. Experimental photophysical data showed that each complex was luminescent in the deep-red region (ca. 680 nm) with corresponding lifetimes indicating the phosphorescent nature of the emission. The influence of the different diimine ligand structures upon the emission wavelengths was minimal, although time-resolved transient absorption data, which supported the triplet assignment of the excited states, did reveal obvious differences between the 2-pyridinyl and 2-pyrazinyl containing complexes.

Experimental Section

All reactions were performed with the use of vacuum line and Schlenk techniques. Reagents were commercial grade and were used without further purification. ^1H, ^{13}C and ^{19}F NMR spectra were recorded on a Bruker Avance dpx 400, or 500 MHz spectrometer, and were recorded in $CDCl_3$, CD_3CN or d6-DMSO solutions. ^1H and $^{13}C\{^1H\}$ NMR chemical shifts (δ) were determined relative to internal tetramethylsilane, $Si(CH_3)_4$ and are given in ppm. Mass spectra were obtained by the staff at Cardiff University. All photoluminescence data was obtained on a JobinYvon-Horiba Fluorolog-3 spectrometer fitted with a JY TBX picosecond photodetection module in MeCN solutions. The pulsed source was a Nano-LED configured for 295 nm output operating at 500 kHz or 1 MHz. Luminescence lifetime profiles were obtained using the JobinYvon-Horiba FluoroHub single photon counting module and the data fits yielded the lifetime values using the provided DAS6 deconvolution software. IR spectra were recorded on an ATR equipped Shimadzu IRAffinity-1 spectrophotometer. UV-vis data were recorded as solutions on a Perkin Elmer Lamda20 spectrophotometer. Transient absorption measurements were carried out using an Edinburgh Instruments LP920 spectrometer. All spectra were collected using a pump

Research Article
doi.org/10.1002/ejic.202300102

wavelength of 355 nm (third harmonic of a Continuum Surelite II Nd:YAG laser system). The probe light for these measurements was a Xenon lamp, affording spectral generation between $300 < \lambda < 800$ nm. Wavelength dependent spectra were recorded with a 2.05 nm spectral resolution, collected using an Andor ICCD camera, and integrated over the first 500 ns after the pump laser pulse. The spectra are presented as $\Delta OD_{Xe\ lamp}$, which is simply referred to as ΔOD. Lifetime data was generated using a photomultiplier to collect time resolved signals, with the bandwidth of these data being identical to the camera resolution (2.05 nm). The lifetime data was fitted using the Origin 2018 software package using a monoexponential function, with no evidence of multiexponential components. Uncertainties in lifetimes are taken from the Least-Squares fitting algorithm, and are not indicative of the uncertainties in multiple fits or data sets.

X-ray crystallography

Data collection and processing

A suitable crystal of $[Ir(1nq)_2(\mathbf{L^1})]PF_6$ was selected and data collected following a standard method,[36] on a Rigaku FRE+ diffractometer equipped with VHF Varimax confocal mirrors, an AFC12 goniometer and HyPix 6000 detector, equipped with an Oxford Cryosystems low-temperature device operating at $T = 100(2)$ K.

Cell determination, data collection, data reduction, cell refinement and absorption correction were carried out using CrysAlisPro[37] The structure was solved with the ShelXT[38] structure solution program using the Intrinsic Phasing solution method and by using Olex2[39] as the graphical interface. The models were refined with version 2018/3 of ShelXL[40] using least squares minimisation.

Deposition Number 2218051 (for [Ir(1nq)2(L1)]PF6) contains the supplementary crystallographic data for this paper. These data are provided free of charge by the joint Cambridge Crystallographic Data Centre and Fachinformationszentrum Karlsruhe Access Structures service.

Computational methods

Electronic structure calculations were all performed using density fitted-density functional theory within the Gaussian 09 computational chemistry suite.[41] All calculations were performed using the Stuttgart-Dresden (SDD) effective core potential and basis set in the treatment of the iridium,[42] in combination with a 6-31G* basis set for all other light atoms.[43] Full geometry optimizations were performed for the cationic complexes utilizing the self-consistent reaction field model (SCRF) which treats the solvent implicitly as a dielectric continuum. In all cases the solvent chosen was acetonitrile, consistent with that utilized in the majority of the spectroscopic measurements. This computational method models the solvent as surrounding a cavity in which the solute resides, and this cavity is characterized using an integral equation formalism for the polarizable continuum model (IEFPCM). This model represents the system in equilibrium during, for example, an optimization routine: in all excited state calculations a non-equilibrium solvent model is used.

All geometry optimizations were performed using an ultrafine grid and very tight convergence criteria, and the minima were confirmed as stationary points through the computation of harmonic vibrational frequencies, each of which showed no imaginary components. These stationary points were used in single point TD-DFT calculations to compute vertical excitation energies. All TD-DFT calculations were undertaken using a linear response approach. All TD-DFT calculations were also performed with a long range corrected hybrid functional (CAM-B3LYP).

Phosphorescence and spin-forbidden absorption bands were investigated using unrestricted density functional theory to compute parameters associated with the first triplet state (T_1), using an identical methodology as for the singlet states. Decomposition of the molecular orbital character was performed using the GaussSum software package.[44] Crystal structure overlays with optimised computational structures has been performed using the Chimera software package, which has also been used to calculate root mean squared deviation (RMSD) values for these comparative structures.[45]

General method for the synthesis of the ligands

The isatin (1 eq.) and either 2-acetylpyridine or 2-acetylpyrazine (1 equiv.) were ground together in a pestle and mortar for 5 min until homogeneous. To this, 33% aqueous NaOH solution (2 mL, 4 eq) was added, and the colour changed immediately from orange to dark red. The mixture was ground for a further 15 min until the solution solidified. The solid was slurried by the addition of cold water (2 mL) and collected onto a sinter, where it was washed with ice water (5 mL). The crude material was then washed with acetone to remove any unreacted isatin and acetyl. The off-white sodium salt was dissolved in water (500 mL) and the solution was neutralised with 5 M HCl, where upon a precipitate appeared. This was collected on a sinter and washed with water before triturating with ethanol (20 mL) to yield the title products as an off-white solid

2-(pyridin-2-yl)quinoline-4-carboxylic acid ($\mathbf{L^1}$)

Synthesised from isatin (1 g, 6.8 mmol) and 2-acetylpyridine (0.823 g, 6.8 mmol) to yield an off-white solid (0.494 g, 35%). Spectral properties agree with those listed in the literature.[27]

6-methoxy-2-(pyridin-2-yl)quinoline-4-carboxylic acid ($\mathbf{L^2}$)

From 5-methoxyisatin (1 g, 5.6 mmol) and 2-acetylpyridine (0.684 g, 5.6 mmol) to yield an off-white solid (0.552 g, 33%). ^{1}H NMR (400 MHz, d_6-DMSO) δ_H 13.81 (br s, 1H), 9.02 (s, 1H), 8.75 (s, 1H), 8.57 (d, J = 7.6 Hz, 1H), 8.25 (s, 1H), 8.15–8.08 (m, 1H), 8.06–7.98 (m, 1H), 7.58–7.48 (m, 2H), 3.94 (s, 3H) ppm. ^{13}C{^{1}H} NMR (101 MHz, d_6-DMSO) δ 167.7, 158.8, 154.6, 152.6, 149.4, 144.5, 137.5, 131.5, 126.2, 124.6, 122.5, 120.6, 119.9, 104.0, 55.5 ppm. UV-vis (0.1 M NaOH): λ_{abs} ($\varepsilon/\times 10^4$ L mol^{-1} cm^{-1}) 256 (2.6), 274 (2.2), 342 (1.0) nm. FTIR (solid) (ATR) ν_{max}: 3143, 3034, 1685 (C=O), 1620, 1598, 1568, 1550, 1508, 1481, 1436, 1408, 1359, 1334, 1269, 1246, 1219, 1186, 1161, 1082, 1047, 1022, 1010, 885, 862, 825, 783, 758, 734, 704, 659, 634, 557, 524, 511, 406 cm^{-1}. HRMS (ES) $[M+H]^+$ Calc'd for $C_{16}H_{13}N_2O_3$ 281.0926; Found *m/z* 281.0930.

6-fluoro-2-(pyridin-2-yl)quinoline-4-carboxylic acid ($\mathbf{L^3}$)

From 5-fluoroisatin (1 g, 6.1 mmol) and 2-acetylpyridine (0.734 g, 6.1 mmol) to yield an off-white solid (0.692 g, 46%). ^{1}H NMR (400 MHz, d_6-DMSO) δ_H 14.05 (br s, 1H), 9.09 (s, 1H), 8.79 (d, J = 4.4 Hz, 1H), 8.64–8.54 (m, 2H), 8.29 (dd, J = 9.3, 5.9 Hz, 1H), 8.06 (dd, J = 8.2, 7.5 Hz, 1H), 7.83 (ddd, J = 9.4, 9.0, 2.5 Hz, 1H), 7.64–7.53 (m, 1H) ppm. ^{19}F{^{1}H} NMR (376 MHz, d_6-DMSO) δ −109.98 (s) ppm.^{13}C {^{1}H} NMR (126 MHz, d_6-DMSO) δ 167.6, 162.4, 160.5, 155.3, 154.6, 150.5, 146.1, 138.1, 133.4, 133.3, 126.2, 125.6, 121.5, 121.0, 121.0, 120.8, 110.0, 109.8 ppm. UV-vis (0.1 M NaOH): λ_{abs} ($\varepsilon/\times 10^4$ L mol^{-1} cm^{-1}) 271 (1.6), 325 (0.7) nm. FTIR (solid) (ATR) ν_{max}: 3109, 3086, 1701 (C=O), 1624, 1600, 1591, 1550, 1508, 1481, 1446,

Research Article
doi.org/10.1002/ejic.202300102

1344, 1327, 1286, 1238, 1211, 1163, 1151, 1101, 1083, 1014, 827, 877, 833, 821, 788, 759, 740, 707, 682, 661, 640, 611, 590, 511, 478, 443, 403 cm^{-1}. HRMS (ES) $[M+H]^+$ Calc'd for $C_{15}H_{10}FN_2O_2$ 269.0726; Found *m/z* 269.0746.

2-(pyrazin-2-yl)quinoline-4-carboxylic acid (L^4)

From isatin (1 g, 6.8 mmol) and 2-acetylpyrazine (0.83 g, 8.8 mmol) to yield an off-white solid (0.456 g, 32%). Spectral properties were in agreement with those listed in the literature.[28]

6-methoxy-2-(pyrazin-2-yl)quinoline-4-carboxylic acid (L^5)

From 5-methoxyisatin (1 g, 5.6 mmol) and 2-acetylpyrazine (0.689 g, 5.6 mmol) to yield an off-white solid (0.803 g, 51%). ^{1}H NMR (400 MHz, d_6-DMSO) δ_H 9.70 (s, 1H), 8.95–8.73 (m, 3H), 8.26 (s,1H), 8.14 (s, 1H), 7.56 (s, 1H), 3.94 (s 3H) ppm.^{13}C{^{1}H} NMR (101 MHz, d_6-DMSO) δ 167.6, 159.0, 150.8, 149.8, 145.2, 144.5, 144.1, 142.5, 131.6, 126.5, 122.8, 119.7, 104.1, 55.6 ppm. UV-vis (0.1 M NaOH): λ_{abs} ($\varepsilon/\times 10^4$ L mol^{-1} cm^{-1}) 257 (2.4), 283 (1.7), 344 (1.4) nm. FTIR (solid) (ATR) ν_{max}: 3120, 3064, 1701 (C=O), 1622, 1527, 1504, 1485, 1438, 1421, 1359, 1338, 1288, 1263, 1226, 1184, 1151, 1089, 1062, 1016, 929, 912, 852, 833, 790, 765, 736, 719, 673, 646, 603, 557, 526, 493, 405 cm^{-1}. HRMS (ES) $[M+H]^+$ Calc'd for $C_{15}H_{12}N_3O_3$ 282.0879; Found *m/z* 282.0882.

6-fluoro-2-(pyrazin-2-yl)quinoline-4-carboxylic acid (L^6)

From 5-fluoroisatin (1 g, 6.1 mmol) and 2-acetylpyrazine (0.740 g, 6.1 mmol) to yield an off-white solid (0.521 g, 34%). ^{1}H NMR (400 MHz, d_6-DMSO) δ_H 14.20 (br s, 1H), 9.74 (s, 1H), 8.98 (s, 1H), 8.83 (dd, J = 8.3, 1.8 Hz, 2H), 8.58 (d, J = 10.7 Hz, 1H), 8.36–8.30 (m, 1H), 7.86 (dd, J = 9.6, 8.2 Hz, 1H) ppm. ^{19}F{^{1}H} NMR (376 MHz, d_6-DMSO) δ −109.09 (s) ppm. ^{13}C NMR (126 MHz, d_6-DMSO) δ 166.9, 162.3, 160.3, 153.1, 153.1, 149.2, 145.8, 145.6, 144.3, 142.89, 136.3, 136.2, 133.1, 133.0, 125.9, 125.8, 120.8, 120.6, 120.5, 109.6, 109.4 ppm. UV-vis (0.1 M NaOH): λ_{abs} ($\varepsilon/\times 10^4$ L mol^{-1} cm^{-1}) 280 (1.5), 319 (1.1) nm. FTIR (solid) (ATR) ν_{max}: 3109, 3072, 1718 (C=O), 1654, 1649, 1622, 1560, 1527, 1508, 1481, 1460, 1421, 1363, 1336, 1325, 1274, 1236, 1226, 1207, 1182, 1145, 1083, 1060, 1016, 935, 916, 881, 852, 833, 790, 763, 738, 723, 673, 646, 547, 503, 489, 437, 420, 408 cm^{-1}. HRMS (ES) $[M+H]^+$ Calc'd for $C_{14}H_9N_3O_2$ 270.0679; Found *m/z* 270.0680.

General procedure for the synthesis of the complexes

$[Ir(1nq)_2(MeCN)_2]BF_4$ was dissolved in chloroform (10 mL). A slight excess of ligand was added and the solution stirred at reflux for 16 h. The solvent was removed and the product purified by silica gel column chromatography, eluting first with DCM followed by DCM/methanol (9:1), collecting the second red fraction.

$[Ir(1nq)_2(L^1)]BF_4$

Obtained from $[Ir(1nq)_2(MeCN)_2]BF_4$ (100 mg, 0.099 mmol) and L^1 (30 mg, 0.12 mmol) to give the product as a red solid (87 mg, 75%). ^{1}H NMR (500 MHz, $CDCl_3$) δ 9.29 (s, 1H), 8.87 (s, 1H), 8.73 (d, *J* = 8.5 Hz, 1H), 8.67 (d, *J* = 8.5 Hz, 1H), 8.43 (d, *J* = 8.6 Hz, 2H), 8.26–8.09 (m, 3H), 8.04 (s, 2H), 7.90 (s, 1H), 7.79 (d, *J* = 8.0 Hz, 1H), 7.74–7.68 (m, 2H), 7.53–7.46 (m, 2H), 7.46–7.40 (m, 2H), 7.40–7.35 (m, 2H), 7.29–7.21 (m, 4H), 7.03 (d, *J* = 8.5 Hz, 1H), 6.96–6.88 (m, 2H), 6.74 (s, 1H), 6.68 (s, 1H), 6.37 (s, 1H), 4.66 (q, *J* = 7.1 Hz, 2H), 4.58–4.39 (m, 2H), 1.59 (t, *J* = 7.2 Hz, 3H), 1.53–1.35 (m, 3H) ppm. ^{13}C NMR (126 MHz, $CDCl_3$) δ 171.9, 170.7, 165.2, 164.7, 149.4, 140.5, 138.0, 137.8, 132.2, 131.9, 131.7, 131.7, 131.3, 130.6, 130.3, 129.9, 128.4, 128.1, 127.8, 127.5, 126.8, 126.4, 126.3, 124.5, 124.2, 123.6, 123.6, 122.9, 121.9, 121.4, 121.2, 62.8, 14.4, 14.2 ppm. UV-vis (MeCN): λ_{abs} ($\varepsilon/\times 10^4$ L mol^{-1} cm^{-1}) 273 (5.0), 368 (1.8), 492 (0.5) nm. FTIR (solid) (ATR) ν_{max}: 1722 (C=O), 1595, 1575, 1533, 1456, 1436, 1325, 1269, 1238, 1195, 1153, 1124, 1099, 1025, 837 (PF_6), 790, 769, 748, 713,657, 557 (PF_6), 497, 445, 432, 412 cm^{-1}. HRMS (ES) $[M-PF_6]^+$ Calc'd for $C_{59}H_{42}N_4O_6Ir$ 1093.2710; Found *m/z* 1093.2697.

$[Ir(1nq)_2(L^2)]BF_4$

Obtained from $[Ir(1nq)_2(MeCN)_2]BF_4$ (50 mg, 0.05 mmol) and L^2 (17 mg, 0.07 mmol) to give the product as a red solid (28 mg, 45%). ^{1}H NMR (500 MHz, $CDCl_3$) δ 9.34 (s, 1H), 8.75 (d, J = 8.6 Hz, 1H), 8.70 (d, J = 7.6 Hz, 1H), 8.48 (d, J = 9.0 Hz, 1H), 8.36 (d, J = 8.3 Hz, 1H), 8.30 (d, J = 8.1 Hz, 1H), 8.13 (d, J = 8.6 Hz, 1H), 8.10 (s, 2H), 8.01 (d, J = 5.5 Hz, 1H), 7.97 (s, J = 9.8 Hz, 1H), 7.95–7.91 (m, 1H), 7.79 (d, J = 7.6 Hz, 1H), 7.73–7.69 (m, 2H), 7.52–7.46 (m, 2H), 7.44–7.40 (m, 1H), 7.39–7.34 (m, 2H), 7.31 (d, J = 9.5 Hz, 1H), 7.26–7.20 (m, 3H), 7.08 (d, J = 8.5 Hz, 1H), 7.04–6.99 (m, 1H), 6.91–6.83 (m, 2H), 6.29 (dd, J = 9.5, 2.7 Hz, 1H), 6.25 (d, J = 8.4 Hz, 1H), 4.66 (q, J = 7.1 Hz, 2H), 4.48 (q, J = 7.1 Hz, 2H), 3.66 (s, 3H), 1.59 (t, J = 7.1 Hz, 3H), 1.38 (t, J = 7.1 Hz, 3H) ppm. ^{13}C NMR (126 MHz, $CDCl_3$) δ 172.0, 171.2, 170.9, 165.4, 165.1, 159.2, 159.1, 153.9, 149.7, 147.6, 147.4, 142.0, 140.7, 140.0, 138.1, 137.8, 136.4, 132.4, 132.3, 132.2, 131.9, 131.8, 131.4, 130.7, 130.6, 130.4, 130.1, 129.8, 128.6, 128.3, 128.0, 128.0, 126.9, 126.7, 126.4, 126.2, 124.6, 124.4, 123.8, 123.8, 123.2, 123.1, 123.0, 121.6, 121.1, 105.9, 63.1, 63.0, 56.0, 14.5, 14.1 ppm. UV-vis (MeCN): λ_{abs} ($\varepsilon/\times 10^4$ L mol^{-1} cm^{-1}) 217 (7.9), 261 (5.6), 285 (4.6), 373 (2.4), 494 (0.5) nm. FTIR (solid) (ATR) ν_{max}: 1716 (C=O), 1614, 1575, 1533, 1506, 1487, 1456, 1436, 1296, 1271, 1234, 1195, 1124, 1099, 1024, 837 (PF_6), 785, 746, 713, 557 (PF_6), 446, 410, 403 cm^{-1}. HRMS (ES) $[M-PF_6]^+$ Calc'd for $C_{60}H_{44}N_4O_7Ir$ 1125.2839; Found *m/z* 1125.2893.

$[Ir(1nq)_2(L^3)]BF_4$

Obtained from $[Ir(1nq)_2(MeCN)_2]BF_4$ (50 mg, 0.05 mmol) and L^3 (17 mg, 0.06 mmol) to give the product as a red solid (47 mg, 76%). ^{1}H NMR (500 MHz, $CDCl_3$) δ 9.33 (s, 1H), 8.75 (d, *J* = 8.6 Hz, 1H), 8.70 (d, *J* = 8.4 Hz, 1H), 8.62 (d, *J* = 9.1 Hz, 1H), 8.45–8.39 (m, 2H), 8.36 (d, *J* = 7.5 Hz, 1H), 8.25 (s, 1H), 8.15 (d, *J* = 8.1 Hz, 1H), 8.06 (d, *J* = 4.8 Hz, 1H), 8.03–7.96 (m, 2H), 7.80 (d, *J* = 7.9 Hz, 1H), 7.75–7.69 (m, 2H), 7.53–7.37 (m, 5H), 7.35–7.30 (m, 2H), 7.28 (s, 1H), 7.23 (s, 1H), 7.09–7.04 (m, 1H), 7.01–6.96 (m, 1H), 6.92–6.81 (m, 2H), 6.44–6.36 (m, 1H), 6.26 (d, *J* = 8.4 Hz, 1H), 4.66 (q, *J* = 7.1 Hz, 2H), 4.55–4.45 (m, 2H), 1.59 (t, *J* = 7.1 Hz, 3H), 1.41 (t, *J* = 6.5 Hz, 3H) ppm. ^{19}F NMR (471 MHz, $CDCl_3$) δ −72.58 (d, *J* = 712.2 Hz, PF_6), −107.98 (s) ppm. ^{13}C NMR (126 MHz, $CDCl_3$) δ 171.9, 165.3, 164.8, 160.0, 149.6, 147.6 140.7, 138.2, 137.8, 132.3, 132.2, 132.1, 131.9, 131.9, 131.5, 130.6, 130.4, 128.6, 128.1, 127.2, 126.6, 126.6, 126.4, 124.7, 124.5, 123.9, 123.8, 123.3, 123.2, 121.6, 121.2, 63.0, 63.0, 14.5, 14.2 ppm. UV-vis (MeCN): λ_{abs} ($\varepsilon/\times 10^4$ L mol^{-1} cm^{-1}) 219 (8.8), 257 (6.6), 361 (2.8), 391 (2.0), 490 (0.6) nm. FTIR (solid) (ATR) ν_{max}: 1720 (C=O), 1595, 1575, 1533, 1498, 1483, 1436, 1384, 1325, 1296, 1269, 1232, 1193, 1153, 1124, 1099, 1024, 937, 891, 839 (PF_6), 785, 746, 711, 665, 624, 557 (PF_6), 518, 493, 472, 433, 410, 403 cm^{-1}. HRMS (ES) $[M-PF_6]^+$ Calc'd for $C_{59}H_{41}N_4O_6FIr$ 1113.2639; Found *m/z* 1113.2689.

$[Ir(1nq)_2(L^4)]BF_4$

Obtained from $[Ir(1nq)_2(MeCN)_2]BF_4$ (100 mg, 0.099 mmol) and L^4 (30 mg, 0.12 mmol) to give the product as a red solid (46 mg, 40%). ^{1}H NMR (500 MHz, $CDCl_3$) δ 9.47 (s, 1H), 9.33 (s, 1H), 8.94 (d, *J* = 8.7 Hz, 1H), 8.75 (d, *J* = 8.5 Hz, 1H), 8.71 (d, *J* = 8.6 Hz, 1H), 8.56 (s, 1H), 8.47 (d, *J* = 8.2 Hz, 1H), 8.37 (d, *J* = 8.9 Hz, 1H), 8.23 (s, 1H), 8.19

(d, J=8.6 Hz, 1H), 8.08 (s, 2H), 7.83 (d, J=7.8 Hz, 1H), 7.77–7.71 (m, 2H), 7.56–7.45 (m, 4H), 7.44–7.37 (m, 3H), 7.34–7.27 (m, 2H), 7.05 (d, J=8.4 Hz, 1H), 6.97 (dd, J=9.4, 8.0 Hz, 1H), 6.90–6.81 (m, 2H), 6.79 (dd, J=8.0, 7.9 Hz, 1H), 6.35 (d, J=8.6 Hz, 1H), 4.67 (q, J=7.2 Hz, 2H), 4.60–4.45 (m, 2H), 1.60 (t, J=7.1 Hz, 3H), 1.50 (t, J=7.0 Hz, 3H) ppm. ^{13}C NMR (126 MHz, $CDCl_3$) δ 171.9, 170.6, 165.2, 165.8, 164.7, 149.2, 147.7, 140.4, 138.6, 137.8, 132.4, 132.2, 132.1, 131.9, 131.6, 131.5, 130.8, 130.5, 130.4, 130.1, 128.8, 128.5, 128.3, 128.2, 128.0, 127.7, 127.0, 126.7, 126.3, 125.0, 124.6, 124.3, 123.8, 123.2, 122.2, 121.6, 121.4, 77.1, 63.1, 63.0, 62.9, 14.5, 14.4 ppm. UV-vis (MeCN): λ_{abs} ($\varepsilon/\times10^4$ L mol^{-1} cm^{-1}) 219 (8.4), 256 (6.3), 349 (2.6), 404 (1.7), 493 (0.6) nm. FTIR (solid) (ATR) ν_{max}: 1716 (C=O), 1683, 1575, 1558, 1533, 1506, 1473, 1456, 1436, 1269, 1234, 1151, 1099, 1024 (BF_4), 891, 813, 767, 748, 518 (BF_4), 443, 432 cm^{-1}. HRMS (ES) $[M-BF_4]^+$ Calc'd for $C_{58}H_{41}N_5O_6Ir$ 1094.2662; Found *m/z* 1094.2663.

$[Ir(1nq)_2(L^5)]BF_4$

Obtained from $[Ir(1nq)_2(MeCN)_2]BF_4$ (50 mg, 0.05 mmol) and L^5 (17 mg, 0.06 mmol) to give the product as a red solid (27 mg, 43 %). ^{1}H NMR (500 MHz, $CDCl_3$) δ 9.44 (s, 1H), 9.29 (s, 1H), 8.72 (d, J=8.7 Hz, 1H), 8.69 (d, J=8.4 Hz, 1H), 8.56–8.35 (m, 5H), 8.34–8.24 (m, 3H), 8.22 (s, 2H), 8.00 (s, 1H), 7.81 (d, J=8.0 Hz, 1H), 7.73 (d, J=8.0 Hz, 1H), 7.72 (d, J=7.9 Hz, 1H), 7.52 (dd, J=9.2, 7.4 Hz, 2H), 7.50–7.44 (m, 1H), 7.44–7.38 (m, 2H), 7.30 (s, 1H), 7.28 (s, 1H), 7.01 (s, 1H), 6.99 (s, 1H), 6.83 (s, 2H), 6.40 (s, 1H), 6.34 (s, 1H), 4.66 (q, J=7.1 Hz, 2H), 4.57–4.48 (m, 2H), 3.85 (s, 3H), 1.59 (t, J=7.1 Hz, 4H), 1.51–1.44 (m, 3H) ppm. ^{13}C NMR (126 MHz, $CDCl_3$) δ 171.9, 170.6, 166.9, 165.2, 164.8, 149.3, 147.4, 147.0, 140.6, 138.5, 137.8, 132.4, 132.2, 132.1, 131.9, 131.6, 130.4, 130.1, 129.6, 128.5, 128.2, 127.3, 126.7, 125.0, 124.6, 123.8, 123.5, 121.7, 121.3, 63.1, 63.0, 56.1, 14.5, 14.2 ppm. UV-vis (MeCN): λ_{abs} ($\varepsilon/\times10^4$ L mol^{-1} cm^{-1}) 217 (6.0), 260 (4.5), 282 (3.5), 356 (1.9), 402 (1.1), 492 (0.4) nm. FTIR (solid) (ATR) ν_{max}: 1734 (C=O), 1716, 1683, 1653, 1647, 1635, 1577, 1558, 1541, 1533, 1508, 1498, 1489, 1473, 1458, 1436, 1419,, 1271, 1232, 1217, 1151, 1022 (BF_4), 835, 669, 518 (BF_4), 472, 457, 433, 418, 412, 403 cm^{-1}. HRMS (ES) $[M-BF_4]^+$ Calc'd for $C_{59}H_{43}N_5O_7Ir$ 1124.2768; Found *m/z* 1124.2789.

$[Ir(1nq)_2(L^6)]BF_4$

Obtained from $[Ir(1nq)_2(MeCN)_2]BF_4$ (40 mg, 0.04 mmol) and L^1 (21 mg, 0.07 mmol) to give the product as a red solid (16 mg, 33 %). ^{1}H NMR (500 MHz, $CDCl_3$) δ 9.53 (s, 1H), 9.34 (s, 1H), 8.80 (d, J=8.4 Hz, 1H), 8.75 (d, J=8.7 Hz, 1H), 8.72 (d, J=8.5 Hz, 1H), 8.58 (s, 1H), 8.44 (d, J=8.0 Hz, 1H), 8.37 (s, 1H), 8.30 (d, J=9.1 Hz, 1H), 8.19 (d, J=8.5 Hz, 1H), 8.08 (s, 2H), 7.83 (d, J=7.9 Hz, 1H), 7.77–7.72 (m, 2H), 7.58–7.51 (m, 3H), 7.48 (d, J=9.8 Hz, 1H), 7.45–7.37 (m, 2H), 7.33–7.27 (m, 2H), 7.06 (d, J=8.5 Hz, 1H), 7.00 (dd, J=10.5, 7.1 Hz, 1H), 6.91–6.84 (m, 1H), 6.81 (d, J=8.5 Hz, 1H), 6.55 (s, 1H), 6.29 (d, J=8.3 Hz, 1H), 4.67 (q, J=7.1 Hz, 2H), 4.60–4.46 (m, 2H), 1.59 (t, J=7.2 Hz, 3H), 1.50 (t, J=6.9 Hz, 3H) ppm. ^{19}F NMR (471 MHz, $CDCl_3$) δ −102.52 (s), −148.01 (s, BF_4) ppm. ^{13}C NMR (126 MHz, $CDCl_3$) δ 171.8, 170.5, 165.0, 164.5, 160.2, 154.0, 149.2, 147.6, 146.7, 143.5, 143.5, 140.7, 140.5, 138.6, 138.1, 137.7, 132.2, 132.0, 131.8, 131.6, 130.4, 130.2, 130.0, 128.8, 128.5, 128.3, 127.9, 126.7, 126.0, 124.9, 124.7, 123.7, 123.2, 121.8, 121.5, 121.3, 63.0, 63.0, 14.4, 14.2 ppm. UV-vis (MeCN): λ_{abs} ($\varepsilon/\times10^4$ L mol^{-1} cm^{-1}) 218 (7.3), 256 (5.1), 355 (2.2), 396 (1.5), 495 (0.5) nm. FTIR (solid) (ATR) ν_{max}: 1718 (C=O), 1593, 1550, 1531, 1498, 1475, 1436, 1382, 1296, 1267, 1236, 1193 (BF_4), 1168, 1151, 1151, 1124, 1099, 1022 (BF_4), 935, 891, 862, 815, 785, 767, 746, 713, 682, 582, 518 (BF_4), 495, 426, 412, 403 cm^{-1}. HRMS (ES) $[M-BF_4]^+$ Calc'd for $C_{58}H_{40}N_5O_6FIr$ 1112.2569; Found *m/z* 1112.2583.

Acknowledgements

Cardiff University (Knowledge Economy Skills Scholarships to C.E.E.) and STG Aerospace are thanked for financial support. We thank the EPSRC UK National Crystallographic Service at the University of Southampton and the Chemistry Department, Jazan University, Saudi Arabia, for financial support and a scholarship to H.Y.O.

Conflict of Interest

The authors declare no conflict of interest.

Data Availability Statement

The data that support the findings of this study are available in the supplementary material of this article.

Keywords: 4-quinolinecarboxylic acid · Cyclometalation · Iridium · Luminescence · Synthesis

[1] *Iridium(III) in Optoelectronic and Photonics Applications*; Zysman-Colman, E., Ed.; John Wiley & Sons, Inc: Chichester, West Sussex, **2017**.
[2] a) K.K.C-W. Lo, D.C.-M. Ng, C.-K. Chung, *Organometallics* **2001**, *20*, 4999; b) Q. Zhao, C. Huang, F. Li, *Chem. Soc. Rev.* **2011**, *40*, 2508; c) E. Baggaley, M. R. Gill, N. H. Green, D. Turton, I. V. Sazanovich, S. W. Botchway, C. Smythe, J. W. Haycock, J. A. Weinstein, J. A. Thomas, *Angew. Chem. Int. Ed.* **2014**, *53*, 3367; d) M. P. Coogan, V. Fernandez-Moreira, *Chem. Commun.* **2014**, *50*, 384; e) L. K. McKenzie, I. V. Sazanovich, E. Baggaley, M. Bonneau, V. Guerchais, J. A. G. Williams, J. A. Weinstein, H. E. Bryant, *Chem. Eur. J.* **2017**, *23*, 234; f) E. Baggely, J. A. Weinstein, J. A. G. Williams, *Struct. Bond.* **2015**, *165*, 205.
[3] a) S. Lamansky, P. Djurovich, D. Murphy, F. Abdel-Razzaq, H.-E. Lee, C. Adachi, P. E. Burrows, S. R. Forrest, M. E. Thompson, *J. Am. Chem. Soc.* **2001**, *123*, 4304; b) D. Ma, R. Liu, C. Zhang, Y. Qiu, L. Duan, *ACS Photonics* **2018**, *5*, 3428; c) D. Ma, C. Zhang, R. Liu, Y. Qiu, L. Duan, *ACS Appl. Mater. Interfaces* **2018**, *10*, 29814; d) D. Tordera, A. Pertegas, N. M. Shavaleev, R. Scopelliti, E. Orti, H. J. Bolink, E. Baranoff, M. Gratzel, M. K. Nazeeruddin, *J. Mater. Chem.* **2012**, *22*, 19264; e) I. N. Mills, J. A. Porras, S. Bernhard, *Acc. Chem. Res.* **2018**, *15*, 352.
[4] a) C. K. Prier, D. A. Rankic, D. W. C. MacMillan, *Chem. Rev.* **2013**, *113*, 5322; b) Z. Zuo, D. T. Ahneman, L. Chu, J. A. Terrett, A. G. Doyle, D. W. C. MacMillan, *Science* **2014**, *345*, 437; c) A. J. Hallet, N. White, W. Wu, X. Cui, P. N. Horton, S. J. Coles, J. Zhao, S. J. A. Pope, *Chem. Commun.* **2012**, *48*, 10838.
[5] Y. Li, N. Dandu, R. Liu, L. Hu, S. Kilina, W. Sun, *ACS Appl. Mater. Interfaces* **2013**, *5*, 6556.
[6] a) S. J. Sheet, B. Sen, S. Khatua, *Inorg. Chem.* **2019**, *58*, 3635; b) W. H.-T. Law, K.-K. Leung, L. C.-C. Lee, C.-S. Poon, H.-W. Liu, K. K.-W. Lo, *ChemMedChem.* **2014**, *9*, 1316; c) K. W.-W. Lo, S. P.-Y. Li, K. Y. Zhang, *New J. Chem.* **2011**, *35*, 265.
[7] a) J. Sun, W. Wu, J. Zhao, *Chem. Eur. J.* **2012**, *18*, 8100; b) T. N. Singh-Rachford, F. N. Castellano, *Coord. Chem. Rev.* **2010**, *254*, 2560; c) X. Guo, Y. Liu, Q. Chen, D. Zhao, Y. Ma, *Adv. Opt. Mater.* **2018**, *6*, 1700981; d) C. Kerzig, O. S. Wenger, *Chem. Sci.* **2018**, *9*, 6670; e) J. Zhao, W. Wu, J. Sun, S. Guo, *Chem. Soc. Rev.* **2013**, *42*, 5323; f) C. E. McCusker, F. N. Castellano, *Top. Curr. Chem.* **2016**, *374*, 19; g) F. N. Castellano, C. E. McCusker, *Dalton Trans.* **2015**, *44*, 17906; h) K. A. Phillips, T. M. Stonelake, K. Chen, Y. Hou, J. Zhao, S. J. Coles, P. N. Horton, S. J. Keane, E. C. Stokes, I. A. Fallis, A. J. Hallett, S. P. O'Kell, J. B. Beames, S. J. A. Pope, *Chem. Eur. J.* **2018**, *24*, 8577.
[8] A. F. Henwood, E. Zysman-Colman, *Chem. Commun.* **2016**, *53*, 807.
[9] a) S. Lamansky, P. Djurovich, D. Murphy, F. Abdel-Razzaq, H. E. Lee, C. Adachi, P. E. Burrows, S. R. Forrest, M. E. Thompson *J. Am. Chem. Soc.*

2001, *123*, 4304; b) A. Tsuboyama, H. Iwawaki, M. Furugori, T. Mukaide, J. Kamatani, S. Igawa, T. Moriyama, S. Miura, T. Takiguchi, S. Okada, M. Hoshino, K. Ueno, *J. Am. Chem. Soc.* **2003**, *125*, 12971.
[10] a) P.-N. Lai, T. S. Teets, *Chem. Eur. J.* **2019**, *25*, 6026; b) P.-N. Lai, Alam, M. K. Brysacz, N. A. Ayoub, T. G. Gray, J. Bao, T. S. Teets, *J. Am. Chem. Soc.* **2018**, *140*, 10198.
[11] F. Monti, A. Baschieri, L. Sambri, N. Armaroli, *Acc. Chem. Res.* **2021**, *54*, 1492.
[12] S. Ladouceur, E. Zysman-Colman, *Eur. J. Inorg. Chem.* **2013**, 2985.
[13] a) E. E. Langdon-Jones, A. J. Hallett, J. D. Routledge, D. A. Crole, B. D. Ward, J. A. Platts, S. J. A. Pope, *Inorg. Chem.* **2013**, *52*, 448; b) T. M. Stonelake, K. A. Phillips, H. Y. Otaif, Z. C. Edwardson, P. N. Horton, S. J. Coles, J. M. Beames, S. J. A. Pope, *Inorg. Chem.* **2020**, *59*, 2266; c) S. A. Fitzgerald, H. Y. Otaif, C. E. Elgar, N. Sawicka, P. N. Horton, S. J. Coles, J. M. Beames, S. J. A. Pope, *Inorg. Chem.* **2021**, *60*, 15467; d) H. Y. Otaif, S. J. Adams, P. N. Horton, S. J. Coles, J. M. Beames, S. J. A. Pope, *RSC Adv.* **2021**, *11*, 39718.
[14] a) D. Schneidenbach, S. Ammermann, M. Debeaux, A, Freund, M. Zollner, C. Daniliuc, P. G. Jones, W. Kowalsky, H.-H. Johannes, *Inorg. Chem.* **2010**, *49*, 397; b) Y.-M. Jing, F.-Z. Wang, Y.-X. Zheng, J.-L. Zuo, *J. Mater. Chem. C* **2017**, *5*, 3714; c) W. Sun, C. Pei, T. Lu, P. Cui, Z. Li, C. McCleese, Y. Fang, S. Kilina, Y. Song, C. Burda, *J. Mater. Chem. C* **2016**, *4*, 5059; d) K. Tani, H. Fujii, L. Mao, H. Sakurai, T. Hirao, *Bull. Chem. Soc. Jpn.* **2007**, *80*, 783.
[15] A. H. Day, M. H. Ubler, H. L. Best, E. Lloyd-Evans, R. J. Mart, I. A. Fallis, R. K. Allemann, E. A. H. Al-Wattar, N. I. Keymer, N. J. Buurma, S. J. A. Pope, *Chem. Sci.* **2020**, *11*, 1599.
[16] a) J. Guo, J. Zhou, G. Fu, Y. He, W. Li, X. Lu, *Inorg. Chem. Commun.* **2019**, *101*, 69; b) C.-J. Li, S.-Y. Yin, H.-P. Wang, Z.-W. Wei, M. J. Pan, *Photochem. Photobiol. A* **2019**, *379*, 99; c) H.-Y. Chen, C.-H. Yang, Y. Chi, Y.-M. Cheng, Y.-S. Yeh, P.-T. Chou, H.-Y. Hsieh, C.-S. Liu, S.-M. Peng, G.-H. Lee, *Can. J. Chem.* **2006**, *84*, 309; d) K. A. Phillips, T. M. Stonelake, P. N. Horton, S. J. Coles, A. J. Hallett, S. P. O'Kell, J. M. Beames, S. J. A. Pope, *J. Organomet. Chem.* **2019**, *893*, 11; e) W. Leslie, R. A. Poole, P. R. Murray, L. J. Yellowlees, A. Beeby, J. A. G. Williams, *Polyhedron* **2004**, *23*, 2769; f) B. Q. Liu, L. Lystrom, C. G. Cameron, S. Kilina, S. A. McFarland, W. F. Sun, *Eur. J. Inorg. Chem.* **2019**, 2208.
[17] C. Kaes, A. Katz, *Chem. Rev.* **2000**, *100*, 3553.
[18] For example, a) C. M. Harris, S. Kokot, H. R. H. Patel, E. Sinn, H. Wong, *Aust. J. Chem.* **1972**, *25*, 1631; b) C. J. O'Connor, E. Sinn, *Inorg. Chem.* **1978**, *17*, 2067; c) M. H. Zaghal, H. A. Qaseer, *Inorg. Chim. Acta* **1989**, *163*, 193.
[19] A. Zucca, D. Cordeschi, L. Maidich, M. I. Pilo, E. Masolo, S. Stoccoro, M. A. Cinellu, S. Galli, *Inorg. Chem.* **2013**, *52*, 7717.
[20] J. T. Madak, C. R. Cuthbertson, Y. Miyata, S. Tamura, E. M. Petrunak, J. A. Stuckey, Y. Han, M. He, D. Sun, H. D. Showalter, N. Neamati, *J. Med. Chem.* **2018**, *61*, 5162.
[21] D. L. Dexter, D. P. Hesson, R. J. Ardecky, G. V. Rao, D. L. Tippett, B. A. Dusak, K. D. Paull, J. Plowman, B. M. DeLarco, V. L. Narayanan, *Cancer Res.* **1985**, *45*, 5563.
[22] For example, a) R. Cody, D. Stewart, M. DeForni, M. Moore, B. Dallaire, N. Azarnia, J. Gyves, *Am. J. Clin. Oncol.* **1993**, *16*, 526; b) J. Maroun, J. Ruckdeschel, R. Natale, R. Morgan, B. Dallaire, R. Sisk, J. Gyves, *Cancer Chemother. Pharmacol.* **1993**, *32*, 64.
[23] Q. Hui, X. Li, W. Fan, C. Gao, L. Zhang, H. Qin, L. Wei, L. Zhang, *Front. Chem.* **2022**, *10*, 880067.
[24] C. E. Elgar, H. Y. Otaif, X. Zhang, J. Zhao, P. N. Horton, S. J. Coles, J. M. Beames, S. J. A. Pope, *Chem. Eur. J.* **2021**, *27*, 3427.
[25] a) J. A. Knight, H. K. Porter, P. K. Calaway, *J. Chem. Soc.* **1944**, *66*, 1893; b) M. G. A. Shvekhgeimer, *Chem. Heterocycl. Compd.* **2004**, *40*, 257.
[26] For example, a) D. B. Patel, D. P. Rajani, S. D. Rajani, H. D. Patel, *J. Heterocycl. Chem.* **2020**, *57*, 1524; b) D. B. Patel, R. H. Vekariya, K. D. Patel, N. P. Prajapati, M. S. Vasava, H. D. Patel, *J. Chem. Pharm. Res.* **2017**, *9*, 216.
[27] Y. Bass, R. J. Morgan, R. J. Donovan, A. D. Baker, *Synth. Commun.* **1997**, *27*, 2165.
[28] A. Shafiee, N. Tavasoli, K. Abdolahnegat, F. Kamal, *J. Sci. Islamic Repub. Iran* **1993**, *4*, 118.
[29] M. Nonoyama, *Bull. Chem. Soc. Jpn.* **1974**, *47*, 767.
[30] For example, a) S. Lamansky, P. Djurovich, D. Murphy, F. Abdel-Razzaq, R. Kwong, I. Tsyba, M. Bortz, B. Mui, R. Bau, M. E. Thompson, *Inorg. Chem.* **2001**, *40*, 1704; b) A. B. Tamayo, B. D. Alleyne, P. I. Djurovich, S. Lamansky, I. Tsyba, N. M. Ho, R. Bau, M. E. Thompson, *J. Am. Chem. Soc.* **2003**, *125*, 7377.
[31] R. A. Smith, E. C. Stokes, E. E. Langdon-Jones, J. A. Platts, B. M. Kariuki, A. J. Hallett, S. J. A. Pope, *Dalton Trans.* **2013**, *42*, 10347.
[32] A. Juris, V. Balzani, F. Barigelletti, S. Campagna, P. Belser, A. von Zelewsky, *Coord. Chem. Rev.* **1988**, *84*, 85.
[33] a) P. N. Lai, T. S. Teets, *Chem. Eur. J.* **2019**, *25*, 6026; b) E. Kabir, Y. Y. Wu, S. Sittel, B. L. Nguyen, T. S. Teets, *Inorg. Chem. Front.* **2020**, *7*, 1362; c) Y. Ha, J. H. Seo, Y. K. Kim, *Synth. Met.* **2008**, *158*, 548; d) P. H. Lanoe, J. Chan, G. Gontard, F. Monti, N. Armaroli, A. Barbieri, H. Amouri, *Eur. J. Inorg. Chem.* **2016**, 1631; e) Y. M. Jing, F. Z. Wang, Y. X. Zheng, J. L. Zuo, *J. Mater. Chem. C* **2017**, *5*, 3714.
[34] a) A. B. Tamayo, S. Garon, T. Sajato, P. I. Djurovich, I. M. Tsyba, R. Bau, M. E. Thompson, *Inorg. Chem.* **2005**, *44*, 8732; b) S. Y. Lee, Y. N. Oh, D. M. Shin, H. K. Kim, *J. Nanosci. Nanotechnol.* **2018**, *18*, 7137; c) M. Lepeltier, F. Dumur, G. Wantz, N. Vila, I. Mbomekalle, D. Bertin, D. Gigmes, C. R. Mayer, *J. Lumin.* **2013**, *143*, 145; d) C. L. Ho, H. Li, W. Y. Wong, *J. Organomet. Chem.* **2014**, *751*, 261; e) H. B. Han, R. Z. Cui, G. Z. Lu, Z. G. Wu, Y. X. Zheng, L. Zhou, H. J. Zhang, *Dalton Trans.* **2017**, *46*, 14916.
[35] F. S. M. Canisares, A. M. G. Mutti, E. F. Santana, V. C. Oliveira, D. G. S. M. Cavalcante, A. E. Job, A. M. Pires, S. A. M. Lima, *Photochem. Photobiol. Sci.* **2022**, *21*, 1077.
[36] S. J. Coles, P. A. Gale, *Chem. Sci.* **2012**, *3*, 683.
[37] CrysAlisPro Software System, Rigaku Oxford Diffraction, **2018**.
[38] G. M. Sheldrick, *Acta Crystallogr.* **2015**, *A71*, 3.
[39] O. V. Dolomanov, L. J. Bourhis, R. J. Gildea, J. A. K. Howard, H. Puschmann, *J. Appl. Crystallogr.* **2009**, *42*, 339.
[40] G. M. Sheldrick, *Acta Crystallogr.* **2015**, *C27*, 3.
[41] M. J. Frisch, G. W. Trucks, H. B. Schlegel, G. E. Scuseria, M. A. Robb, J. R. Cheeseman, G. Scalmani, V. Barone, G. A. Petersson, H. Nakatsuji, X. Li, M. Caricato, A. Marenich, J. Bloino, B. G. Janesko, R. Gomperts, B. Mennucci, H. P. Hratchian, J. V. Ortiz, A. F. Izmaylov, J. L. Sonnenberg, D. Williams-Young, F. Ding, F. Lipparini, F. Egidi, J. 33 Goings, B. Peng, A. Petrone, T. Henderson, D. Ranasinghe, V. G. Zakrzewski, J. Gao, N. Rega, G. Zheng, W. Liang, M. Hada, M. Ehara, K. Toyota, R. Fukuda, J. Hasegawa, M. Ishida, T. Nakajima, Y. Honda, O. Kitao, H. Nakai, T. Vreven, K. Throssell, J. A. Montgomery, Jr., J. E. Peralta, F. Ogliaro, M. Bearpark, J. J. Heyd, E. Brothers, K. N. Kudin, V. N. Staroverov, T. Keith, R. Kobayashi, J. Normand, K. Raghavachari, A. Rendell, J. C. Burant, S. S. Iyengar, J. Tomasi, M. Cossi, J. M. Millam, M. Klene, C. Adamo, R. Cammi, J. W. Ochterski, R. L. Martin, K. Morokuma, O. Farkas, J. B. Foresman, D. J. Fox, *Gaussian 09, Revision C.01*, Gaussian Inc., Wallingford CT, **2016**.
[42] a) T. H. Dunning Jr., P. J. Hay, in *Modern Theoretical Chemistry*, *Ed. Schaefer III*, *H. F. Vol. 3* (Plenum, New York, **1977**) 1–28; b) W. Kuechle, M. Dolg, H. Stoll, H. Preuss, *Mol. Phys.* **1991**, *74*, 1245.
[43] R. Ditchfield, W. J. Hehre, J. A. Pople, *J. Chem. Phys.* **1971**, *54*, 724.
[44] N. M. O'Boyle, A. L. Tenderholt, K. M. Langner, *J. Comput. Chem.* **2008**, *29*, 839.
[45] E. F. Pettersen, T. D. Goddard, C. C. Huang, G. S. Couch, D. M. Greenblatt, E. C. Meng, T. E. Ferrin, *J. Comput. Chem.* **2004**, *25*, 1605.

Manuscript received: February 23, 2023
Revised manuscript received: March 28, 2023
Accepted manuscript online: April 11, 2023